Seungmoon Choi
chois@purdue.edu
Haptic Interface Research Laboratory
Purdue University
Electrical Engineering Building
465 Northwestern Avenue
West Lafayette, IN 47907

Hong Z. Tan
hongtan@purdue.edu
Haptic Interface Research Laboratory
Purdue University
Electrical Engineering Building
465 Northwestern Avenue
West Lafayette, IN 47907

Perceived Instability of Virtual Haptic Texture. I. Experimental Studies

Abstract

This paper presents a quantitative characterization of the instability that a human user often experiences while interacting with a virtual textured surface rendered with a force-reflecting haptic interface. First, we quantified the degree of stability/instability during haptic texture rendering through psychophysical experiments. The stiffness of the virtual textured surface upon detection of instability was measured under a variety of experimental conditions using two texture rendering methods, two exploration modes, and various texture model parameters. We found that the range of stiffness values for stable texture rendering was quite limited. Second, we investigated the attributes of the proximal stimuli experienced by a human hand while exploring the virtual textured surface in an attempt to identify the sources of perceived instability. Position, force, and acceleration were measured and then analyzed in the frequency domain. The results were characterized by sensation levels in terms of spectral intensity in dB relative to the human detection threshold at the same frequency. We found that the spectral bands responsible for texture and instability perception were well separated in frequency such that they excited different mechanoreceptors and were, therefore, perceptually distinctive. Furthermore, we identified the high-frequency dynamics of the device to be a likely source of perceived instability. Our work has implications for displaying textured surfaces through a force feedback device in a virtual environment.

1 Introduction

Haptic texture rendering is a growing research field that holds much promise for enriching the sensory attributes of objects in a virtual environment and for allowing precise and systematic control of textured surfaces for psychophysical studies. Our long-term research objectives are to have a better understanding of how to characterize surface textures in physical and perceptual spaces and to develop procedure-based rendering algorithms that can effectively span the human perceptual space for haptic texture. The first problem that we have encountered is the instability perceived by a human user while interacting with a virtual textured surface rendered with a force-reflecting haptic interface. This problem has also been reported anecdotally by other researchers (see, for example, Wall & Harwin, 2000; Weisenberger, Krier, & Rinker, 2000). Given the increasingly popular use of force feedback devices for rendering virtual textures, it is imperative that we have a better understanding of the conditions under which haptic virtual textures are free of any unin-

Presence, *Vol. 13, No. 4, August 2004,* 395–415
© 2004 by the Massachusetts Institute of Technology

tended perceptual artifacts. We use the term "perceived instability" to denote any unrealistic sensations (such as buzzing or apparent aliveness of a surface) that can not be attributed to the physical properties of the texture under examination.

Although everyone has some notion of what texture is, the concept of texture is not clearly defined. Katz considered texture as the fine structure of a surface (microgeometry) and as independent of the shape (macrogeometry) of an object or surface (Katz, 1925/1989). The systematic study of haptic texture perception began about thirty years ago (Lederman & Taylor, 1972). One topic that has been controversial is whether information about surface texture is encoded spatially or temporally. Both types of information are available during direct (fingerpad) exploration, but only temporal cues (vibrations) are available during indirect (probe-mediated) exploration. The consensus that has emerged from psychophysical and neurophysiological studies is that humans use temporal cues while exploring surface textures via a probe. While the same temporal cues are available during fingerpad exploration, humans prefer to use intensive (depth of microstructures) and/or spatial (size of microstructures) cues instead (Johnson & Hsiao, 1992). Performance with a bare fingerpad was better for tasks requiring spatial judgments such as haptic object recognition, but roughness perception was very similar whether the direct or the indirect method was used (Lederman & Klatzky, 1999). Recently, Lederman and her colleagues have found that exploration speed has a substantial effect on texture perception, thereby supporting a theory based on temporal coding of texture (Lederman, Klatzky, Hamilton, & Ramsay, 1999). In addition, neurophysiological and psychophysical data suggest that temporal cues are responsible for perception of very fine surface details (with inter-element spacing below 1 mm) (LaMotte & Srinivasan, 1991; Johnson & Hsiao, 1994; Hollins & Risner, 2000). For very smooth surfaces, the probe method produced greater perceived roughness than the fingerpad method (Klatzky & Lederman, 1999). Therefore, probe-mediated surface texture perception should yield results similar to the direct method, with better performance expected for very small-scale (less than 1 mm) surface features.

From the above discussions, it is evident that force-feedback devices that emulate probe-mediated texture exploration should produce successful rendering of textured surfaces. Indeed, the development of computational methods for texture rendering, that is, virtual environment dynamics models for textures, has received increased attention from the haptics research community in the past few years. Minsky's Sandpaper system was perhaps the first successful attempt at generating synthetic textures (Minsky, 1995; Minsky & Lederman, 1996). Using a two degree-of-freedom (DoF) force-reflecting joystick, Minsky developed a tangential force-gradient algorithm for 2D texture rendering, where the displayed force was in the plane of the textured surface and proportional to the gradient of the surface-height profile. Several successful implementations of texture rendering methods using three (or more) DoF force-reflecting devices have also been reported. For 3D haptic rendering, resistive forces are rendered to prevent the penetration of an interaction tool into the objects, thereby conveying the shape of virtual objects. To add a sense of surface texture, variations are imposed on these baseline resistive forces. Massie reported that changing the magnitude of the resistive forces alone can generate the perception of textures (Massie, 1996). Ho, Basdogan, and Srinivasan (1999) developed more sophisticated texture rendering algorithms by using the bump mapping technique in computer graphics to add perturbations to both the magnitude and direction of the resistive forces for various texture models. Other researchers have applied stochastic texture models (Fritz & Barner, 1996; Siira & Pai, 1996; Costa & Cutkosky, 2000; Kim, Kyrikou, Sukhatme, & Desbrun, 2002) and vibration-based models to haptic texture rendering (Okamura, Dennerlein, & Howe, 1998). Most studies on haptic texture rendering have focused on the development of efficient algorithms that are fast enough (with an update rate of 1 kHz or higher) for haptic rendering. These algorithms can potentially produce virtual textures with well-controlled surface characteristics and thus lend themselves well to perceptual studies on texture. To the best of our knowledge, however, few studies have investigated the conditions under which hapti-

cally rendered textures are guaranteed to be perceptually "clean" (i.e., free of artifacts).

In general, there are two major sources of perceived instability during haptic texture rendering: an improper environment model, and unstable control of the haptic interface. Realistic texture rendering requires the environment model to faithfully follow the physical properties of the objects being rendered. In practice, however, the environment model is usually an approximation to the underlying physics, with the goal of inducing a target percept such as the roughness of a textured surface. To the extent that such simplification induces perceptual artifacts, the user can perceive a virtual surface to be unrealistic or unstable. The stability of the haptic interface in a control sense is also a necessary condition for realistic rendering. Perception of buzzing and chattering are likely caused by control instability. Unbounded behavior of a controller, unmodeled dynamics of a haptic interface, quantization noise of encoders, energy instilling effects of a zero-order-hold converter, and asynchronous switch time can all lead to control instability (Gillespie & Cutkosky, 1996). Although many control theoretical studies have tackled the stability problem of virtual walls using a simplified one-DoF interaction model (Gillespie & Cutkosky, 1996; Adams & Hannaford, 1999; Miller, Colgate, & Freeman, 2000; Hannaford, Ryu, & Kim, 2001; Hannaford & Ryu, 2002), these techniques cannot be easily extended to the investigation of the stability of haptic texture rendering. Doing so requires modeling haptic interaction as a multi-DoF problem and extending the surface model from a single flat surface to complex curved surfaces, thereby significantly increasing the complexity of the analysis.

Any study of perceived instability has to take into account the effect of both environment modeling and control stability. In addition, the human decision process also plays a role in the perceived quality of virtual textures. The experiments reported in this paper were designed to address the following two questions with human subjects:

- Under what conditions do human users perceive instability from virtual haptic textures rendered with a force feedback device?
- What are the proximal stimuli that are responsible for the perception of instability, and why?

In the first set of experiments, we quantified the maximum rendering stiffness under which virtual textures are perceived to be realistic. We conducted psychophysical experiments using various texture model parameters, texture rendering methods, and exploration modes. Qualitative descriptions of different kinds of instability were also collected in these experiments. In the second set of experiments, we identified the proximal stimuli that caused the perception of instability. This was accomplished through measurements and analyses of the signals recorded on the stylus that interfaced the human hand with the haptic interface. Some of the results have been published earlier in Choi and Tan (2002a, 2002b).

The remainder of this paper is organized as follows: The methods that are common to both psychophysical and measurement experiments are laid out in section 2. The specific methods and results for the psychophysical experiments are presented in section 3. Those for measurement experiments can be found in section 4. We conclude the paper with a general discussion in section 5.

2 Rendering and Exploration of Virtual Textures Used in Our Experiments

In this section, we provide the details of the texture model, rendering methods, and exploration modes used in both psychophysical and measurement experiments.

2.1 Texture Model

The virtual textured surfaces were modeled as 1D sinusoidal gratings superimposed on a flat surface. This underlying flat surface, defined by $z = 0$ in the world coordinate frame of the PHANToM, formed a vertical wall facing the user of the PHANToM (see Figure 1). The sinusoidal grating was described by

$$z = A \sin([2\pi L]x) + A,$$

where A and L denote the amplitude and (spatial) wave-

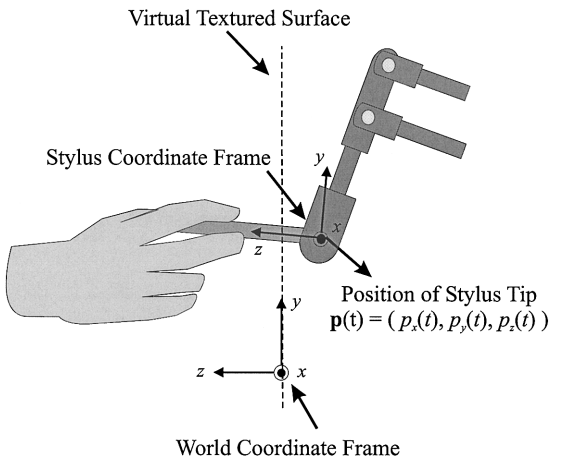

Figure 1. *An illustration of the virtual textured surfaces and the two coordinate frames used in our experiments. Position of the stylus tip was always measured in the world coordinate frame.*

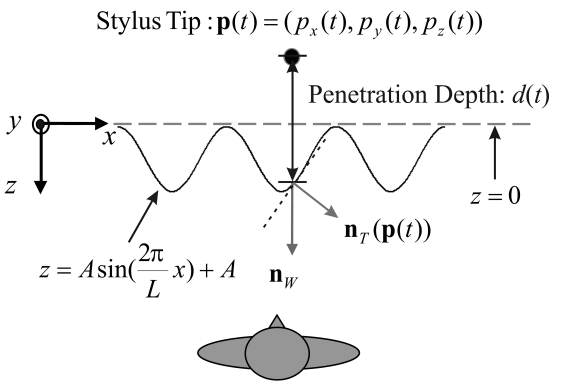

Figure 2. *An illustration of the parameters used in texture rendering.*

length, respectively (see Figure 2). Sinusoidal gratings have been widely used as the basic building blocks for textured surfaces for studies on haptic texture perception (Lederman et al., 1999; Weisenberger et al., 2000). They have also been used as the basis of a function set for modeling real haptic textures (Wall & Harwin, 1999).

2.2 Texture Rendering Method

Two basic texture rendering methods were employed in the current study. Both methods use a spring model to calculate the magnitude of the rendered force as $K \cdot d(t)$, where K is the stiffness of the textured surface, and $d(t)$ is the penetration depth of the stylus at time t (see Figure 2). The penetration depth is calculated as follows:

$$d(t) = \begin{cases} 0 & \text{if } p_z(t) > 0 \\ A \sin(2\pi\, p_x(t/L)) + A - p_z(t) & \text{if } p_z(t) \le 0 \end{cases}, \quad (1)$$

where $p(t) = (p_x(t), p_y(t), p_z(t))$ is the position of the tip of the stylus.

The two methods differ in the way the force directions are rendered. The first method, introduced by Massie (1996), renders a force $\mathbf{F}_{mag}(t)$ with a constant direction normal to the underlying flat wall of the textured surface. The second method, proposed by Ho et al. (1999), renders a force $\mathbf{F}_{vec}(t)$ with varying directions such that it remains normal to the local microgeometry of the sinusoidal texture model. Mathematically,

$$\mathbf{F}_{mag}(t) = Kd(t)\, \mathbf{n}_W, \quad (2)$$

$$\mathbf{F}_{vec}(t) = Kd(t)\, \mathbf{n}_T(\mathbf{p}(t)), \quad (3)$$

where $\mathbf{n}_W$ is the normal vector of the underlying flat wall, and $\mathbf{n}_T(\mathbf{p}(t))$ is the normal vector of the textured surface at $\mathbf{p}(t)$. Both methods keep the force vectors in the horizontal plane (zx plane in Figure 1), thereby eliminating the effect of gravity on rendered forces.

The two texture rendering methods are natural extensions of virtual flat wall rendering techniques. Perceptually, they are very different: textures rendered by $\mathbf{F}_{vec}(t)$ feel rougher than those rendered by $\mathbf{F}_{mag}(t)$ with the same texture model. Textures rendered by $\mathbf{F}_{vec}(t)$ can also feel sticky sometimes.

2.3 Exploration Mode

An exploration mode refers to a stereotypical pattern of the motions that humans employ to perceive a certain object attribute through haptic interaction (Lederman & Klatzky, 1987). In our experiments, we tested two exploration modes, free exploration and stroking, to examine the effect of user interaction patterns on instability perception. In the free exploration mode, subjects were allowed to use the interaction pattern that

they found most effective at discovering instability of virtual textures. This mode was selected to be the most challenging interaction pattern for a haptic texture rendering system in terms of perceived instability. In the stroking mode, subjects were instructed to move the stylus laterally across the textured surface (i.e., along the x axis as shown in Figure 1). Stroking is the exploration mode most frequently employed by humans for texture perception and identification (Lederman & Klatzky, 1987).

3 Psychophysical Experiments

In this section, we describe the experimental design and results of the psychophysical experiments conducted for a quantitative analysis of perceived instability during haptic texture rendering. The specific objectives of these experiments were (1) to quantify the parameter space that results in virtual textures that are perceived to be stable, and (2) to gather qualitative descriptions of different kinds of perceived instability.

3.1 Experiment Design

3.1.1 Apparatus. A PHANToM force-reflecting haptic interface (model 1.0A, SensAble Technologies, Woburn, MA) was used in all experiments to render virtual textured surfaces. It was equipped with a stylus as an interaction tool and encoder gimbals for orientation sensing. This PHANToM model has a nominal positional resolution of 0.03 mm, and a nominal maximum stiffness of 3.5 N/mm.

3.1.2 Stimuli. The virtual texture models used in the experiments had two parameters, amplitude A and wavelength L, of the 1D sinusoidal gratings. Three values of A (0.5, 1.0, and 2.0 mm) and three values of L (1.0, 2.0, and 4.0 mm) were tested, resulting in a total of nine textured surface profiles. These sinusoidal gratings can be well constructed due to the 0.03 mm nominal positional resolution of the PHANToM. Each surface profile was rendered with the two texture rendering methods described in Equations 2 and 3, with stiffness K as the parameter. It follows that the three parameters, A, L, and K, along with the texture rendering methods, uniquely defined the stimuli used in this study.

Due to the fact that the PHANToM workspace boundary exhibits inferior dynamics performance, the virtual textured surface was restricted to a 15 cm $\times$ 15 cm region located near the center of the PHANToM workspace.

3.1.3 Subjects. Three subjects participated in these experiments. One subject (S1, male) was an experienced user of the PHANToM haptic interface. The other two subjects (S2 and S3, females) had not used any haptic interface prior to this study. The average age of the subjects was 26.3 years old. All subjects are right-handed and reported no known sensory or motor abnormalities with their upper extremities.

3.1.4 Conditions. The independent variables employed in the experiments were texture rendering method, exploration mode, and amplitude and wavelength values of sinusoidal surface profiles. Four experiments, defined by the combinations of the two texture rendering methods and the two exploration modes, were conducted. There were nine conditions (3 A $\times$ 3 L values) per experiment (see Table 1).

The dependent variable measured in all 36 experimental conditions (4 experiments $\times$ 9 conditions per experiment) was the maximum stiffness K_T below which the rendered textured surface was perceived to be stable.

3.1.5 Procedure. All subjects went through initial training to develop criteria for the perception of instability of a virtual textured surface. During the training, the subject chose the texture rendering method and selected the values of A, L, and K. The subject was informed that the virtual textures were rendered as 1D sinusoidal gratings. The subject was instructed to regard any sensation that felt unrealistic based on his or her experience of real textures as an indication of perceived instability. Each subject spent approximately one hour on training.

The method of limits (Gescheider, 1985) was used in all experiments. Given a pair of A and L values within

Table 1. *Experimental Conditions for Psychophysical Experiments*

Experiment	Texture rendering method	Exploration mode	A (mm)	L (mm)
I	$\mathbf{F}_{mag}(t)$	Free exploration	.5, 1.0, 2.0	1.0, 2.0, 4.0
II	$\mathbf{F}_{mag}(t)$	Stroking	.5, 1.0, 2.0	1.0, 2.0, 4.0
III	$\mathbf{F}_{vec}(t)$	Free exploration	.5, 1.0, 2.0	1.0, 2.0, 4.0
IV	$\mathbf{F}_{vec}(t)$	Stroking	.5, 1.0, 2.0	1.0, 2.0, 4.0

each of the four experiments, a total of 100 series of trials (50 ascending series and 50 descending series) were conducted. Each ascending series started with a stiffness value of $K_{min} = 0.0$ N/mm (i.e., no force) that was always perceived to be stable. The subject would respond "stable" (by pressing a designated key on the keyboard). The K value was then increased by $\Delta K = 0.02$ N/mm. The subject would feel the virtual textured surface again and respond "stable" or "unstable" according to the perception. As long as the subject chose to report "stable," the K value was incremented by the same ΔK amount for each subsequent trial. An ascending series was terminated when the subject reversed the response from "stable" to "unstable." The value of $K + \Delta K/2$ was then recorded as the estimated threshold for this ascending series, where K was the stiffness of the last trial with a "stable" response.

Each descending series started with a stiffness value of $K_{max} = 0.6$ N/mm. This value was selected based on the preliminary finding that no textured surface felt stable at this K value. The same step size of $\Delta K = 0.02$ N/mm was used to decrease K values in each subsequent trial. A descending series was terminated when the subject reversed the response from "unstable" to "stable." The value of $K - \Delta K/2$ was then recorded as the estimated threshold for this descending series, where K was the stiffness of the last trial with an "unstable" response. With these chosen values of K_{min}, K_{max}, and ΔK, each ascending-descending series could last up to 31 trials.

The experiments proceeded as follows. Each subject performed all nine conditions (3 A values $\times$ 3 L values) in Experiment I first, followed by those in Experiments II, III, and IV. The order of the nine conditions within each experiment was randomized for each subject. For each pair of A and L values, the order of the 50 ascending and 50 descending series was also randomized.

During all experiments, subjects wore headphones with white noise to block the auditory cues emanating from the PHANToM. No visual rendering of the textured surface was provided. Instead, the computer monitor displayed only text information on the current series number.

The following instructions were given to the subjects during all experiments. They were asked to hold the stylus lightly, and to hold it like a pen. For the free exploration mode (Experiments I and III), the subjects were asked to detect any sensations indicating instability using whatever interaction style they had chosen. For the stroking mode (Experiments II and IV), the subjects were instructed to concentrate on the detection of sensations indicating instability while they moved the stylus back and forth along the x direction across the textured surface. They were asked to maintain a constant stroking velocity to the best of their ability.

Typically, it took about an hour for a subject to finish one experimental condition. Each subject finished two or three experimental conditions per day. It took a total of approximately 36 hours for each subject to complete the 36 experimental conditions. A 10 minute break was enforced after a subject had completed the 100 ascending-descending series associated with one experimental condition. This was necessary in order to prevent a carryover effect (i.e., surfaces presented after a series of particularly unstable conditions might have been judged as more stable in a subsequent experiment). Subjects were also allowed to take a break whenever it was needed.

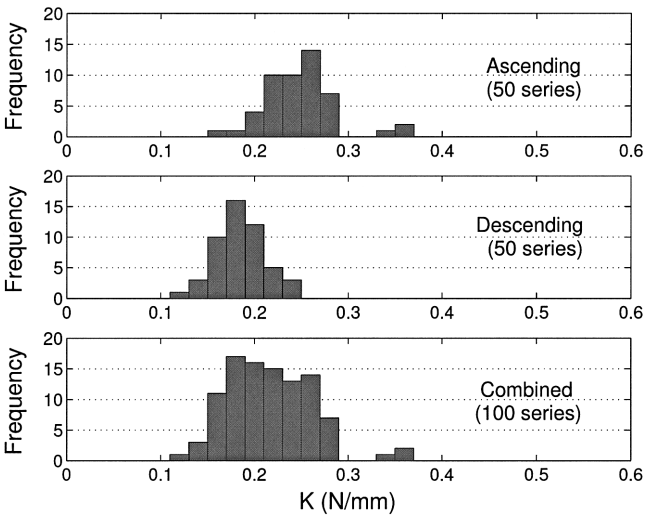

Figure 3. *Typical histograms for one experimental condition (Experiment II, subject S1, A = 2.0 mm, L = 2.0 mm) using the method of limits.*

3.1.6 Stability of Nontextured Flat Wall. After the completion of the main experiments, one subject (S1) was tested with a nontextured flat wall using the same procedure as described above. The result of this test served as a baseline value for stiffness threshold K_T.

3.2 Results

As discussed earlier, 50 ascending and 50 descending series were conducted for each experimental condition (i.e., each pair of A and L values within a main experiment). Figure 3 shows typical results for one experimental condition (subject S1, $\mathbf{F}_{mag}(t)$, stroking, $A = 2.0$ mm, $L = 2.0$ mm). The top panel shows the histogram for all 50 ascending series, the middle panel for all 50 descending series, and the bottom panel for combined series. The average of K values from the 50 ascending series (0.26 N/mm) was greater than that from the descending series (0.19 N/mm). This is typical and reflects what is termed the "errors of habituation" (Gescheider, 1985). It is a common practice to compute the mean from the combined data (0.23 N/mm) and regard it as an estimate of the stiffness threshold K_T.

Results from Experiment 1 ($\mathbf{F}_{mag}(t)$, free exploration) are shown in Figure 4 for the three subjects in separate panels. In each panel, the stiffness thresholds are indicated by squares at their respective A and L values. The mesh shows the fitted surface computed by linear regression analysis (see Equation 4). To help the reader visualize the spatial relationship between threshold data points (squares) and the fitted surface (mesh), straight lines are drawn between the centers of data points and the corresponding points on the mesh with the same A and L values. The standard errors are not indicated in the figures because they were very small (the average standard error was 0.004 N/mm). The volume under the mesh represents the parameter space within which all virtual textured surfaces were perceived to be stable. As can be seen from Figure 4, these volumes were quite small for all subjects. Subject S2 produced the largest volume for stable texture rendering and S3 the smallest. Recall that subject S1 was the only one who was experienced with the PHANToM device. Therefore, prior experience with a force-reflective haptic interface did not necessarily result in a particularly stringent or lenient criterion for judging the stability of virtual textured surfaces.

A five-way ANOVA analysis (subject, texture rendering method, exploration mode, A, and L) showed that there were significant differences among the three subjects tested [$F(2, 10791) = 484.57$, $p < .0001$]. However, since all three plots in Figure 4 exhibited the same general trends, data from all subjects were pooled and summarized in panel (a) of Figure 5. Also shown in Figure 5 are the results from Experiments II, III, and IV in panels (b), (c), and (d), respectively. Overall, the values of K_T ranged from 0.0138 N/mm to 0.4527 N/mm for all the conditions tested. These values were quite small and the resulting textured surfaces felt very soft (like corduroy). They were also much smaller than the stiffness threshold measured with a nontextured wall (1.005 ± 0.157 N/mm for subject S1). The effect of exploration mode can be observed by comparing panel (a) with (b), and (c) with (d). The thresholds associated with the stroking mode [panels (b) and (d)] were larger than those associated with the free-exploration mode [panels (a) and (c)] by an average difference of 0.137

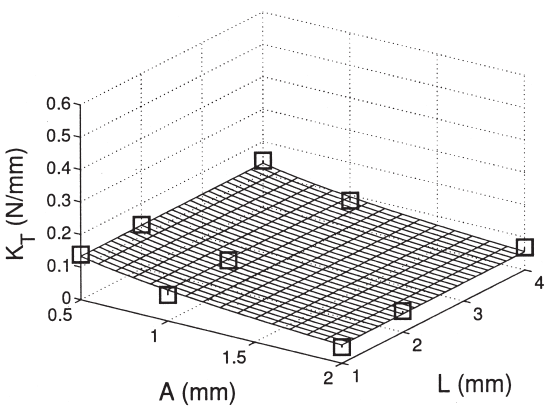

(a) Subject S1

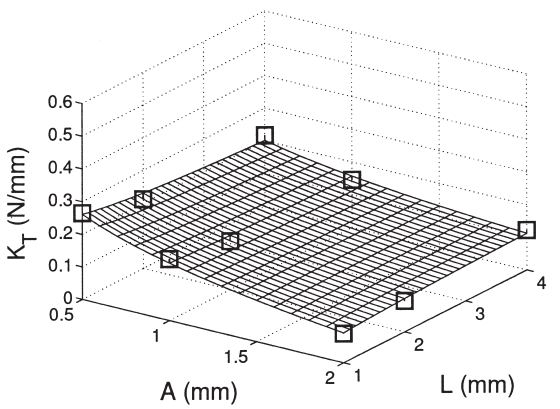

(b) Subject S2

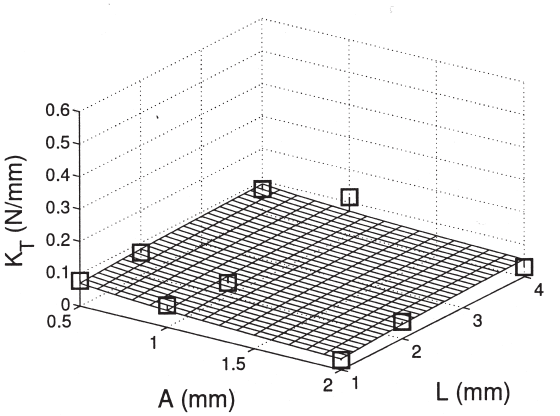

(c) Subject S3

Figure 4. *Experimental results of Experiment I for all subjects. The stiffness thresholds* K_T *are indicated by squares. Regression surfaces representing the boundary of* K_T *for perceptually stable texture rendering are also shown. A solid line is drawn between the center of a datum point and the corresponding point on the regression surface with the same* A *and* L *values to help visualize the position of the datum point.*

N/mm [$F(1, 10764) = 5980.13$, $p < .0001$]. The thresholds for surfaces rendered with the $\mathbf{F}_{\text{mag}}(t)$ method [panels (a) and (b)] were statistically greater than those with the $\mathbf{F}_{\text{vec}}(t)$ method [panels (c) and (d)] by an average difference of 0.099 N/mm [$F(1, 10764) = 3103.44$, $p < .0001$].

The functional relationships between (A, L) and K_T were estimated using the following form of a fitted equation:

$$\hat{K}_T = \beta_0 + \beta_A \log_2 A + \beta_L \log_2 L + \beta_{AL} \log_2 A \cdot \log_2 L. \quad (4)$$

The estimated coefficients are listed in Table 2 for all experiments. They were computed by linear regression analysis for K_T with two log-scaled continuous variables ($\log_2 A$ and $\log_2 L$) and two categorical variables (texture rendering method and exploration mode) as well as their interaction terms ($R^2 = 0.5908$; R^2 is relatively small because we pooled the data of three subjects whose results were significantly different). Note that the nonsignificant coefficients are set to zero in this table.

The effects of the amplitude (A) and wavelength (L) of the sinusoidal gratings on the stiffness threshold K_T can be observed from Figure 5 and Table 2. In Experiments I and II, it is evident from Figure 5 that K_T decreased as A increased. The wavelength (L) had an effect on K_T only through the interaction term $\log_2 A \cdot \log_2 L$, but its effect was very small compared to that of A ($\beta_L = 0.0$, $|\beta_{AL}| \ll |\beta_A|$). In Experiments III and IV, increasing A or L tended to result in lower or higher K_T, respectively, unless K_T was very small, and their interaction was more apparent ($|\beta_{AL}|$ of Experiments III and IV $\gg |\beta_{AL}|$ of Experiments I and II).

Subject debriefing revealed several types of perceived instability during haptic texture rendering. In the free exploration mode, subjects reported that they perceived three types of apparent instabilities: *entry instability*, *inside instability*, and *ridge instability*. These terms reflect the position of the stylus tip where the corresponding type of instability was perceived. Entry instability refers to the phenomenon that as the stylus approached a point on the $z = 0$ plane (see Figure 1), a high-frequency buzzing of the stylus sometimes occurred.

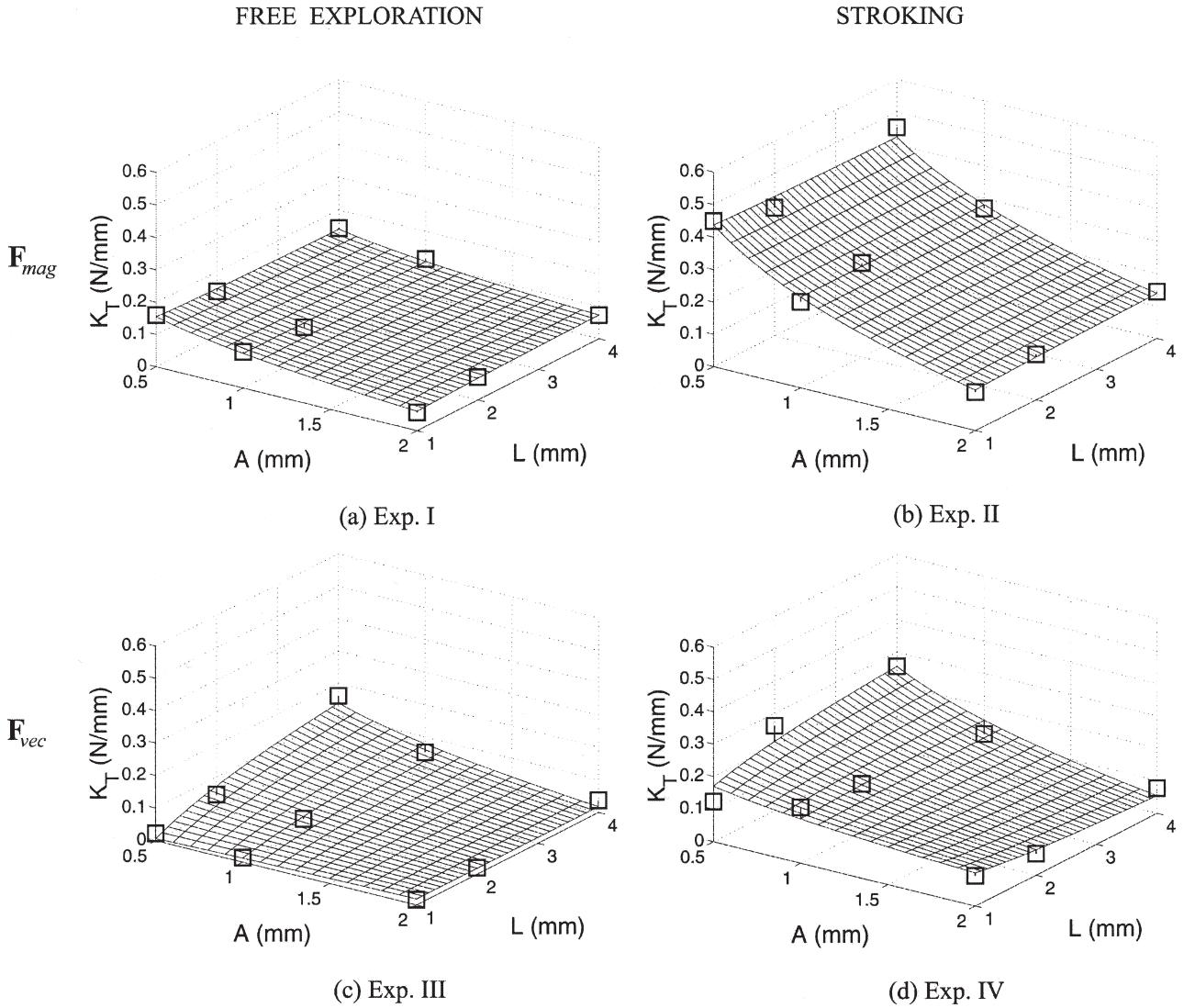

Figure 5. *Results of psychophysical experiments. The stiffness thresholds averaged over all three subjects are shown with open squares. Regression surfaces representing the boundary of* K_T *for perceptually stable texture rendering are shown with meshes. To help the reader visualize the position of the data, a solid line is drawn between the center of each datum point and the corresponding point on the regression surface with the same* A *and* L *values.*

Inside instability was frequently associated with the action of poking. It was most evident when the stylus was pushed deep into a virtual textured surface rendered with $\mathbf{F}_{vec}(t)$. Ridge instability occurred when the stylus was pushed by the PHANToM into the valley of a sinusoidal grating while the subject tried to maintain its position on a ridge of the grating. The subjects also re-

Table 2. *Coefficients of Fitted Regression Equation*

Experiment	β_0	β_A	β_L	β_{AL}
I	.107	−.048	0	.007
II	.281	−.156	0	.007
III	.012	.007	.033	−.033
IV	.136	−.034	.010	−.033

ported that entry and inside instabilities were more pronounced than ridge instability, and therefore they mainly focused on the first two types of instability. In the stroking mode, the textured surface was perceived to be unstable when the subject felt a buzzing noise in addition to the vibrations resulting from the sinusoidal gratings being stroked across.

3.3 Discussion

In the psychophysical experiments, we measured the parameter space within which the subjects did not perceive any instability associated with the virtual textures. We tested two texture rendering methods using sinusoidal gratings and two exploration modes. The maximum stiffness values under which no instability was perceived turned out to be in the range of 0.0138 to 0.4527 N/mm. This range corresponded to surfaces that were soft and spongy to the touch. The stiffness threshold was much smaller than that of a flat surface with no texture (1.005 N/mm).

Our finding that stroking resulted in a larger stiffness threshold than free exploration for the same rendering parameters is to be expected. We recall that our subjects rarely used stroking in the free exploration mode although it was allowed. Instead, they chose to position the stylus at various locations on or inside the virtual textured surface to focus on the detection of any buzzing as an indication of instability. Therefore, in the free exploration mode, the subjects concentrated on the detection of vibrations in the absence of any other signals. In the stroking mode, the subjects always felt the vibration due to the stylus stroking the virtual textured surface. They had to detect additional noise in order to declare the textured surface to be unstable. Due to possible masking of buzzing noise by the vibrations coming from the textured surface, it is conceivable that subjects were not able to detect instability with stroking as easily as they could with static positioning of the stylus (free exploration). In fact, the subjects reported that the experiments with stroking were more difficult to perform. Therefore, textured surfaces explored by stroking appeared to be more stable than those explored by poking or static contact.

Our finding that textures rendered with $\mathbf{F}_{mag}(t)$ resulted in a larger stiffness threshold than those rendered with $\mathbf{F}_{vec}(t)$ is also consistent with the nature of these two rendering methods. While $\mathbf{F}_{mag}(t)$ imposed perturbations in the magnitudes of rendered forces only, $\mathbf{F}_{vec}(t)$ resulted in perturbations in both the directions and the magnitudes of rendered forces. The sometimes abrupt changes in force direction could cause virtual textures rendered with $\mathbf{F}_{vec}(t)$ to be perceived as less stable than those rendered with $\mathbf{F}_{mag}(t)$. To circumvent this problem, Ho, Basdogan, and Srinivasan (1999), who originally proposed the $\mathbf{F}_{vec}(t)$ rendering method, have developed a heuristic algorithm that interpolates the direction of a force vector between the normal to the texture model and the normal to the underlying surface.

To gain intuition into the effects of A or L on K_T, we consider the derivative of the magnitude of the rendered force. Let $g(t) = |\mathbf{F}_{mag}(t)| = |\mathbf{F}_{vec}(t)|$, and assume that the stylus is in contact with the textured surface. From Equations 1 to 3, we have

$$g(t) = K\left[A \sin\left(\frac{2\pi}{L} p_x(t)\right) + A - p_z(t)\right]. \qquad (5)$$

Differentiating $g(t)$ with respect to the time variable t results in

$$\dot{g}(t) = 2\pi \frac{KA}{L} \cos\left(\frac{2\pi}{L} p_x(t)\right) \dot{p}_x(t) - K\,\dot{p}_z(t). \qquad (6)$$

There are two terms in this equation that determine the rate of change in the force magnitude. The term on the right, $K\,\dot{p}_z(t)$, responds to stylus motion in a direction that is normal to the underlying plane $[\dot{p}_z(t)]$ with a gain of K. This is the same term that has been used in formulating the virtual wall (with no texture) problem. The term on the left is due to textures on the virtual wall. Here, the lateral velocity of the stylus $[\dot{p}_x(t)]$ is amplified with three constant gains (K, A, and $1/L$) and one variable gain that depends on the stylus position in the lateral direction $[p_x(t)]$. Increasing A or decreasing L results in a faster change in force magnitude, which can cause a textured surface to be perceived as less stable, or equivalently, result in a smaller stiffness threshold K_T.

Of the three types of instability discovered by the subjects, the sensation associated with entry and inside instability was that of buzzing and vibration. The entry instability was commonly observed for both texture rendering methods. This instability may have resulted from the collision detection algorithm used in the experiments. The collision detection algorithm declares a collision when the PHANToM stylus enters the underlying plane. Thus, the penetration depth computed following Equation 1 included step changes when the stylus entered and left the textured plane, and these step changes may have caused the perception of entry instability. Despite this known problem, this collision detection algorithm is a basic and useful method that can be easily generalized to complex textured objects (see Choi & Tan, 2003, for details).

The inside instability frequently observed in textures rendered with $\mathbf{F}_{vec}(t)$ seems to be consistent with the nature of the texture rendering method. When the stylus is positioned deep inside the texture surface, $\mathbf{F}_{vec}(t)$ generates forces with relatively large magnitudes and fast direction changes. This may have invoked the generation of a high-frequency signal that the subjects described as buzzing.

The sensation associated with ridge instability was qualitatively different and was likely due to the inaccurate environment model of the textured surface. When a real stylus rests on the ridge of a real surface with sinusoidal gratings, the reaction force and friction of the surface combine to counterbalance the force exerted by the user's hand on the stylus, thereby creating an equilibrium. The force rendered by $\mathbf{F}_{vec}(t)$, however, was determined solely on the local texture geometry and did not take into account the direction of user applied force. This is illustrated in Figure 6, where it is assumed that the force applied by the user was normal to the plane underneath the texture. According to the environment model, the force applied by the PHANToM was always in the direction of the surface normal $\mathbf{n}_T(\mathbf{p}(t))$. As a result, the net force exerted on the tip of the stylus (the sum of the forces applied by the user and the PHANToM) was directed towards the valley of the sinusoidal grating. Therefore, the subject who tried to rest the stylus on the ridge could feel the stylus being actively pushed into the valley.

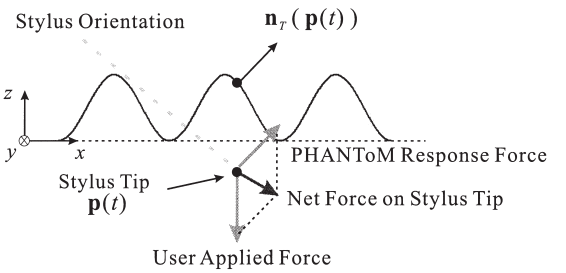

Figure 6. *An illustration of the forces involved in ridge instability.*

In summary, the results of the psychophysical experiments showed that the parameter space for stable texture rendering was too limited to be useful for virtual environment applications or psychophysical studies. As mentioned earlier, the textured surfaces within the stable rendering-parameter range felt like soft corduroy. We were not able to render harder or rougher textured surfaces without inducing the perception of instability. It was therefore necessary to investigate the characteristics and sources of signals that gave rise to perceived instability, with the goal of eliminating them in order to increase the useful parameter space for stable texture rendering.

4 Measurement Experiment

In this section, we report the results on the measurement of the proximal stimuli (position of the tip of the stylus, force, and acceleration) delivered to a subject's hand during the exploration of virtual textures. The specific objectives of this experiment were: (1) to isolate signals responsible for perceived instability; (2) to identify the signal components responsible for the perception of texture and instability, respectively; (3) to analyze the intensity of the proximal stimuli in both physical and perceptual units, and (4) to investigate the sources of signals causing the perception of instability.

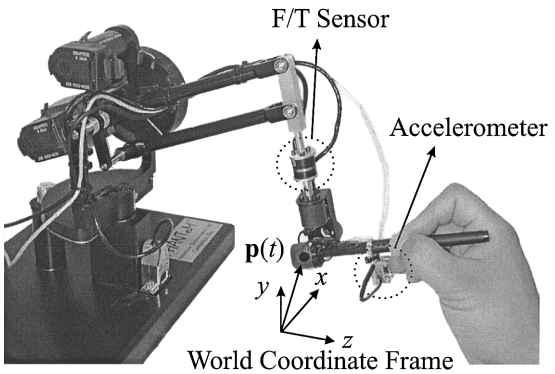

Figure 7. *The PHANToM instrumented with a triaxial F/T sensor and an accelerometer.*

4.1 Experiment Design

4.1.1 Apparatus. The PHANToM force-reflecting device was used for both texture rendering and data collection. The position of the tip of the stylus, $\mathbf{p}(t)$, was measured using the position-sensing routines in the GHOST library provided with the PHANToM. These routines read the optical encoders to sense joint angles of the PHANToM and converted them to a position of the stylus tip in the world coordinate frame.

For force and acceleration measurement, the PHANToM was instrumented with two additional sensors. A triaxial force/torque (F/T) sensor (ATI Industrial Automation, Apex, NC; model Nano 17 with temperature compensation) was used to measure force delivered by the PHANToM, $\mathbf{f}(t)$. In order to minimize the structural change to the PHANToM, a new link with a built-in interface for the F/T sensor was fabricated to replace the last link (i.e., the link closest to the stylus) of the PHANToM (see Figure 7). The new link was of the same length as the original one, but weighed 60 g (13%) more. Force data were transformed into the stylus coordinate frame. The origin of the stylus coordinate frame was always located at the tip of the stylus (i.e., $\mathbf{p}(t)$), and its z-axis coincides with the cylindrical axis of the stylus (see Figure 1).

Acceleration of the stylus was captured with a triaxial accelerometer (Kistler, Blairsville, PA; model 8794A500). The accelerometer was attached through a rigid mount that was press-fitted to the stylus. The attachment added 11.8 g to the weight of the stylus. Acceleration measurements, $\mathbf{a}(t)$, were also taken in the stylus coordinate frame.

The effects of the sensor attachments on the device performance were investigated in terms of apparent inertia at the PHANToM stylus. We measured the tip inertia of the original and instrumented PHANToM devices along paths that passed the origin of the PHANToM coordinate frame. Two paths were chosen to be parallel to one of the axes of the PHANToM coordinate frame, differing in the direction of tip movement during the measurements (a total of six paths). The results are summarized in Table 3. It turned out that the tip inertia along the y-axis was affected most significantly by the the addition of the two sensors. In particular, the apparent tip inertia in the $-y$ direction (the direction of gravity) was reduced by 139.4 g. This was due to the fact that the additional sensor weight increased the effect of gravity on the corresponding tip inertia. The inertia along other directions changed in the range 13.8–29.4 g, and were therefore much less affected by the additional sensor weight. Since the forces used in our experiments for rendering textured surfaces were confined in the x-z plane, we concluded, based on these measurements, that the instrumented PHANToM was able to reproduce the stimuli that led to perceived instability during the psychophysical experiments conducted earlier.

4.1.2 Subjects. Two subjects participated in the measurement experiment (one male, S1, and one female, S4). Their average age was 33 years old. Both are right-handed and report no known sensory or motor abnormalities with their upper extremities. Only S1 had participated in the previous psychophysical experiments.

Both subjects were experienced users of the PHANToM device. They were preferred over naive subjects because our experiments required the subjects to place or move the stylus in a particular manner in order to maintain well-controlled conditions during data collection.

4.1.3 Experimental Conditions. A total of seven experimental conditions was employed (see Table

Table 3. *Comparison of Apparent Tip Inertia of the Original and Instrumented PHANToM Devices*

Tip movement direction	Original PHANToM tip inertia (g)	Instrumented PHANToM tip inertia (g)	Effect of sensor attachment
$+x$	222.6	208.8	13.8 g decrease
$-x$	245.4	224.0	21.4 g decrease
$+y$	236.0	278.8	42.8 g increase
$-y$	282.4	143.0	139.4 g decrease
$+z$	97.2	126.6	29.4 g increase
$-z$	114.8	101.0	13.8 g decrease

Table 4. *Experimental Conditions for Measurement Experiment*

Exploration mode	Texture rendering method	Perceptual category	Texture model parameters A (mm), L (mm), K (N/mm)
Free exploration	$\mathbf{F}_{mag}(t)$	Entry instability	1, 2, .30
Free exploration	$\mathbf{F}_{vec}(t)$	Entry instability	1, 2, .30
Free exploration	$\mathbf{F}_{vec}(t)$	Inside instability	1, 2, .05
Stroking	$\mathbf{F}_{mag}(t)$	Stable	1, 2, .15
Stroking	$\mathbf{F}_{mag}(t)$	Unstable	1, 2, .40
Stroking	$\mathbf{F}_{vec}(t)$	Stable	1, 2, .15
Stroking	$\mathbf{F}_{vec}(t)$	Unstable	1, 2, .40

4). In the conditions using free exploration, we collected data for the two primary instability categories of entry and inside instability. Note that inside instability with $\mathbf{F}_{mag}(t)$ was not tested because this type of instability had not been observed during our previous psychophysical experiments. For stroking, we recorded data under both stable and unstable conditions. Both texture rendering methods were tested for the stroking mode.

Whether a particular experimental condition resulted in the perception of instability depended on the values of the rendering parameters (A, L, and K). The values listed in Table 4 were selected based on the results obtained from our previous psychophysical experiments (see Figure 5). We chose stiffness values that were either one standard deviation below the measured stiffness thresholds (for stable conditions) or one standard deviation above the thresholds (for unstable conditions).

4.1.4 Procedures. For the experiments with the free exploration mode, the subjects were instructed to hold the stylus still, near the textured surface (entry instability) or deep inside the textured surface (inside instability). They had to find a point in space where the surface was clearly perceived to be unstable and maintain that position. Once the subject was satisfied with the selected stylus position, the experimenter initiated data collection.

For the experiments with the stroking mode, the subjects were instructed to move the stylus laterally across the virtual gratings. They were required to maintain a constant stroking speed to the best of their ability. After the subject had initiated stroking, the experimenter started data collection.

In all experimental conditions, the subjects were asked to hold the stylus like a pen (see Figure 7). Dur-

ing each trial, 3D position, force, and acceleration data were collected for 10 seconds at a sampling rate of 1 kHz.

4.1.5 Data Analysis. Each 10-sec long time-domain signal was processed as follows. Ten spectral densities corresponding to the ten 1-sec segments of the signal were computed and averaged for noise reduction. We used a flat-top window for the precise recovery of the magnitude of each spectral component (Smith, 1999). The frequency and magnitude of each prominent spectral component in its corresponding physical units were then calculated.

In order to assess the perceived intensities of these spectral peaks, we compared their intensities in physical units to published human detection thresholds for sinusoidal movements. The human detection thresholds for vibrotactile stimuli depend on many factors, including body site and contact area (Bolanowski, Gesheider, Verrillo, & Checkosky, 1988). In our experiments, the stylus was in contact with the distal pads of three fingers (thumb, index finger, and middle finger), and the web between the thumb and the index finger. We therefore compared our measurements to the detection thresholds taken at the distal pad of the middle finger (Verrillo, 1971) and at the thenar eminence (Verrillo, 1963). For both sets of data, we chose the threshold data taken with contactor areas that are closest to our experimental setup (0.3 cm^2 for finger tip and 1.3 cm^2 for thenar eminence). It turned out that the threshold curves from these two body sites are quite similar at their respectively chosen contact areas. We therefore used the detection thresholds for the thenar eminence at 1.3 cm^2 (Verrillo, 1963) for our data analysis. The perceived magnitude of a given spectral peak from the recorded signals was computed as the difference between the log of its intensity and the log of the human detection threshold at the same frequency. As is the common practice in psychophysics literature, these perceived magnitudes are expressed in dB SL (sensation level).

For the stroking mode, we estimated the location of the spectral peak corresponding to texture information as follows. Suppose that a subject explored the textured wall by moving the stylus along the x-axis (see Figure 2) with a constant velocity of v_x, while maintaining contact with the textured surface. Then, the magnitude of the rendered force could be decomposed into two terms. From Equations 2 and 3,

$$|\mathbf{F}_{mag}(t)| = |\mathbf{F}_{vec}(t)| = \left|KA \sin\left(2\pi\frac{v_x}{L}t\right) + K(A - p_z(t))\right|, \tag{7}$$

assuming that $p_x(0) = 0$. The left term delivered the texture signal at frequency v_x/L, and the right term prevented the penetration of the stylus into the textured surface. Therefore, $\hat{f}_{tex}$, the estimated frequency for the spectral component responsible for texture perception, was

$$\hat{f}_{tex} = \frac{\overline{|v_x|}}{L}, \tag{8}$$

where $\overline{|v_x|}$ was the average stroking velocity.

4.2 Results

As an example of the collected data, the experimental results for stable stroking using $\mathbf{F}_{mag}(t)$ are shown in Figure 8 for subject S4. Figures 8(a), 8(b), and 8(c) represent the position, force, and acceleration measurements, respectively. In each figure, the measured 3D time-domain data are plotted in the upper panel, and the corresponding power spectral densities are shown in the lower panel. Note that the power spectral densities below 10 Hz are not shown because they are likely to be 1/f noises.[1] The predicted location ($\hat{f}_{tex}$) of the spectral component for texture information computed using Equation 8 was 50 Hz for this data set. As expected, all spectral densities in Figure 8 showed spectral peaks around 50–60 Hz. We therefore infer that the mechanical energy in this frequency band was indeed responsible for the perception of the desired virtual texture. It was also observed that no prominent

1. $1/f$ noise refers to a noise that starts at 0 Hz and rapidly decays as frequency increases. This noise is very commonly observed in measured data (Smith, 1999).

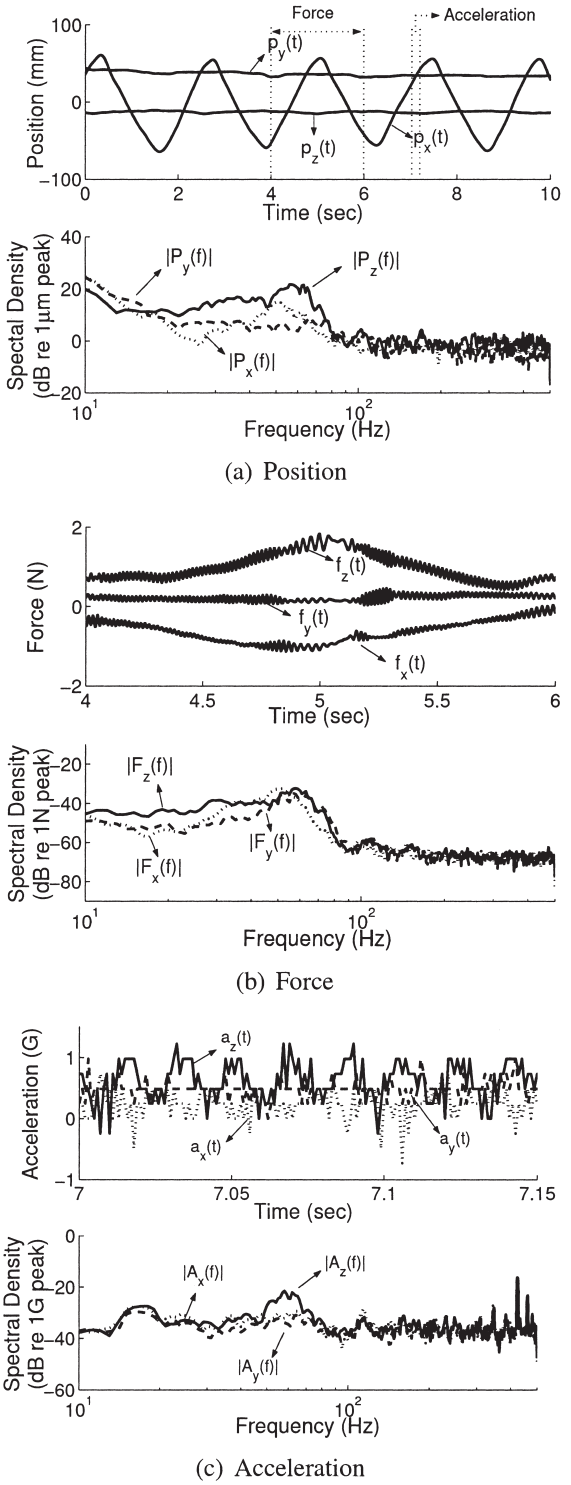

Figure 8. *Experimental data for stable stroking (**F**$_{mag}$(t), subject S4). The measured time-domain data are shown in the upper panels, and their power spectral densities in the lower panels. The corresponding segments of Figure 8(b) (force) and 8(c) (acceleration) are indicated in Figure 8(a) (position).*

peaks appear at higher frequencies for this condition. Furthermore, the locations of the distinct peaks measured with all three sensors were highly consistent, except for the high-frequency noise in the accelerometer data caused by quantization error. This consistency across sensor measurements turned out to be true for all experimental conditions. We therefore report only results obtained from the position data $p_z(t)$ in the remainder of this paper. Note that $p_z(t)$ showed the largest power spectral density among the three positional variables, due to the fact that the normal vector of the underlying flat wall was in the z direction (see Figure 1).

For the free exploration conditions where all renderings were perceived to be unstable, the power spectral densities of $p_z(t)$ exhibited prominent spectral peaks in the frequency range 192–240 Hz. An example of such data (inside instability, $\mathbf{F}_{vec}(t)$, subject S1) is shown in Figure 9(a). The upper panel contains the spectral density function (solid line) along with the detection thresholds taken from Verrillo's work (Verrillo, 1963) (filled triangles) and the linearly-interpolated threshold curve (dotted line). The lower panel shows the difference between the power spectral density and the detection threshold curve. The dotted line indicates the reference line for 0 dB SL. In both panels, a vertical solid line is drawn to locate the peak in the spectral density function. We observe that only the signal components around the spectral peak are significantly above the corresponding absolute detection thresholds. This fact was common to all experimental data for free exploration. It follows that the energy in this high-frequency band (denoted by f_{ins}) was responsible for the perception of instability.

For the stroking data, the predicted frequency $\hat{f}_{tex}$ for texture perception (see Equation 8) was used to locate its corresponding actual spectral peak (f_{tex}) in the recorded data. The results in Table 5 show a close agreement between the values of $\hat{f}_{tex}$ and f_{tex}, with an average prediction error of 5.5 Hz. Recall that $\hat{f}_{tex}$ was estimated under the assumption that the subject moved the stylus with a constant stroking velocity. This may have been the main source of discrepancy between the predicted and measured values of f_{tex}.

In the data measured under the conditions for per-

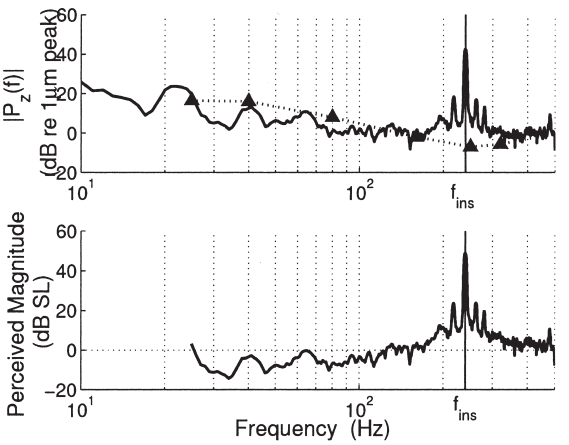

(a) Inside instability, $\mathbf{F}_{vec}(t)$, subject S1

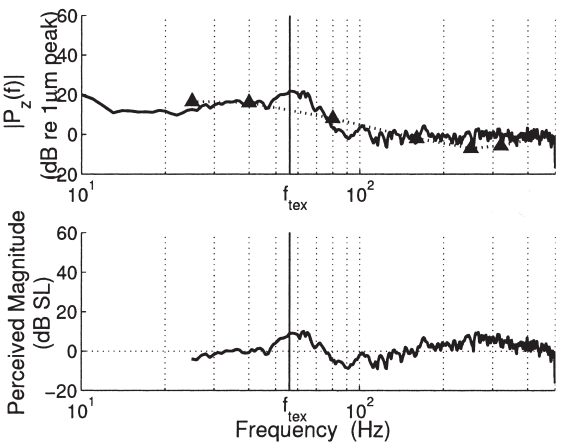

(b) Stable stroking, $\mathbf{F}_{mag}(t)$, subject S4

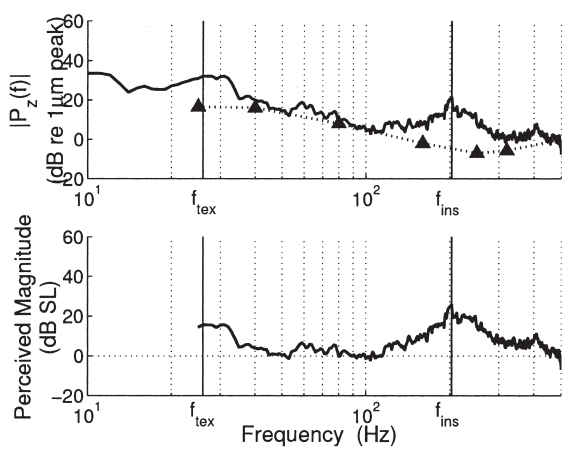

(c) Unstable stroking, $\mathbf{F}_{mag}(t)$, subject S1

Table 5. *Predicted and Measured Locations of the Spectral Peaks for Texture Perception*

Condition and subject	$\hat{f}_{tex}$ (Hz)	f_{tex} (Hz)
Stable stroking, $\mathbf{F}_{mag}(t)$:		
S1	40	51
S4	50	56
Unstable stroking, $\mathbf{F}_{mag}(t)$:		
S1	29	26
S4	39	41
Stable stroking, $\mathbf{F}_{vec}(t)$:		
S1	37	40
S4	57	62
Unstable stroking, $\mathbf{F}_{vec}(t)$:		
S1	21	26
S4	56	65

ceptually stable stroking, only one spectral component that delivered texture information appeared in the power spectral densities. An example is shown in Figure 9(b) ($\mathbf{F}_{mag}(t)$, subject S4). Note that only one spectral peak at 56 Hz (i.e., texture information) appears in this figure.

For the conditions under which the subjects felt instability during stroking, usually two distinctive spectral components were observed in the measured power spectral densities of $p_z(t)$. Figure 9(c) shows an example ($\mathbf{F}_{mag}(t)$, subject S1) of such cases. This spectral density function shows two prominent peaks at f_{tex} = 26 Hz (texture information) and f_{ins} = 203 Hz (perception of instability).

Finally, the perceived magnitudes of spectral components at f_{tex} and f_{ins} are summarized in Table 6 for every

Figure 9. *Average power spectral density of* $p_z(t)$ *and their corresponding sensation levels. The upper panels show the spectral densities (solid lines) with the detection thresholds at the thenar eminence (triangles and dashed lines). The lower panels show the sensation levels as the difference between spectral densities and detection thresholds. The vertical lines mark the spectral components for texture perception* (f_{tex}) *and for perceived instability* (f_{ins}).

Table 6. *Intensities of Spectral Peaks (in Sensation Level) at Frequencies for Texture Perception (f_{tex}) and Instability Perception (f_{ins})*

Condition and subject	SL (dB) @ f_{tex} (Hz)	SL (dB) @ f_{ins} (Hz)
Entry instability, $\mathbf{F}_{mag}(t)$:		
S1	—	39.31 @ 223
S4	—	33.48 @ 221
Entry instability, $\mathbf{F}_{vec}(t)$:		
S1	—	47.84 @ 238
S4	—	33.01 @ 192
Inside instability, $\mathbf{F}_{vec}(t)$:		
S1	—	48.79 @ 240
S4	—	30.92 @ 205
Stable stroking, $\mathbf{F}_{mag}(t)$:		
S1	4.95 @ 51	—
S4	8.91 @ 56	—
Unstable stroking, $\mathbf{F}_{mag}(t)$:		
S1	15.67 @ 26	25.89 @ 203
S4	10.98 @ 41	25.57 @ 194
Stable stroking, $\mathbf{F}_{vec}(t)$:		
S1	8.28 @ 40	—
S4	13.83 @ 62	—
Unstable stroking, $\mathbf{F}_{vec}(t)$:		
S1	8.73 @ 26	21.21 @ 208
S4	23.61 @ 65	26.53 @ 203

experimental condition and every subject. The average values of f_{tex} and f_{ins} were 45.9 and 213.7 Hz, respectively. The range of f_{tex} (26–65 Hz) was well separated from that of f_{ins} (192–240 Hz). Perceived magnitudes ranged from 4.95 to 23.61 dB SL for f_{tex} components and 21.21 to 48.79 dB SL for f_{ins} components, respectively.

4.3 Discussion

In these experiments, we measured position, force, and acceleration signals experienced by the human hand during exploration of virtual textures. Data were recorded for free exploration and stroking modes using two rendering methods under both stable and unstable rendering conditions. As we stated earlier, our first goal was to isolate signal components responsible for the perception of instability. From our psychophysical experiments conducted earlier, we learned that subjects relied on the detection of a "buzzing" vibration to declare a virtual textured surface to be unstable. This indicated a signal with spectral components above 100 Hz (Tan, 1996). Indeed, we were able to isolate signal components in the frequency range of 192–240 Hz from the measurements taken during unstable texture rendering conditions. This happens to be the frequency range at which humans are most sensitive to vibrational stimulation (Bolanowski et al., 1988). From the measurement experiments, we were also able to predict, then locate the spectral components responsible for tex-

ture information in the frequency range of 26–65 Hz. Stimulation in this frequency range is usually perceived to be "rough" and "fluttering" (Mountcastle, Talbot, Darian-Smith, & Kornhuber, 1955). In order to characterize the perceptual intensities of measured signals, the magnitudes of their spectral peaks were converted to perceived magnitudes in dB SL. While the intensities of the signals conveying texture information were of intermediate magnitude (4.95–23.61 dB SL), the high-frequency noises that gave rise to the perception of instability were generally "louder" (21.21–48.79 dB SL) in terms of perception.[2]

The frequency ranges for texture and instability perception are not only well separated in their numerical values, but in the neural mechanism mediating their perception as well. From an engineering point of view, one of the most important performance criteria for any stabilization technique for haptic rendering is the minimization of the loss of perceptual information due to stabilization (Hollerbach & Johnson, 2000). The fact that the two frequency ranges responsible for texture and instability perception are numerically well separated suggests that it ought to be possible to filter out the high-frequency spectral components responsible for instability perception without significantly altering the signals containing texture information. From a perception point of view, it is well established in haptic perception literature that two mechanoreceptive afferent types, the slowly adapting type 1 and the Pacinian system, are responsible for the perception of signals in the 26–65 Hz and the 192–240 Hz frequency ranges, respectively (Bolanowski et al., 1988; Johnson, Yoshioka, & Vega-Bermudez, 2000). When signals in these two frequency regions are combined, they remain perceptually salient and distinctive. Therefore, our subjects were able to simultaneously perceive the spectral peaks responsible for texture and instability.

In an attempt to locate the sources of the high-frequency signals responsible for perceived instability, we measured a z-axis open-loop frequency response of the PHANToM with the tip of the stylus resting at the origin of its world coordinate frame. During the measurement, the stylus was supported by a tight string anchored from above which served to constrain the stylus to point towards the $+z$-direction. The stylus of the PHANToM could only move along the z-axis. This frequency response is defined as

$$|H_z(f)| = \left| \frac{P_z(f)}{\tilde{F}_z(f)} \right|, \qquad (9)$$

where $\tilde{F}_z(f)$ is the Fourier transform of the z-axis force command to the PHANToM, and $P_z(f)$ is the Fourier transform of the z-axis position of the stylus tip. The result, shown in Figure 10, indicates a mechanical resonance at 218 Hz. A similar resonance frequency has also been reported recently for model 1.5 of the PHANToM (Çavuşoğlu, Feygin, & Tendick, 2002). This resonance is well within the 192–240 Hz frequency range. Therefore, it seems to be the source of the spectral peaks in the frequency range that we had identified to be responsible for instability perception. Since humans are most sensitive to vibrations within this frequency range, noise produced by this resonance tends to be "loud" perceptually.

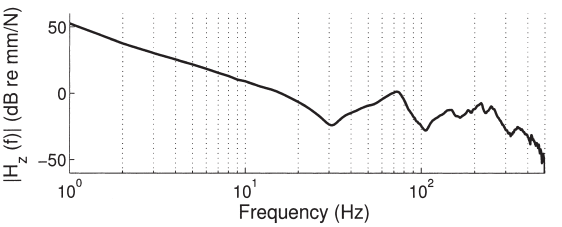

Figure 10. *Frequency response of the PHANToM (model 1.0A) measured at the origin and along the z-axis of its world coordinate frame.*

5 General Discussion

We investigated the problem of *perceived instability* during haptic texture rendering with the aims to quantify conditions under which virtual textures are perceived to be stable, to discover types of perceived insta-

2. According to Verrillo and Gescheider (1992), stimulation levels exceeding 50–55 dB SL start to induce discomfort and fatigue.

bility, and to understand the sources of perceived instability. Our work was performed in the context of applying virtual textures to object surfaces rendered with a force-reflecting haptic interface, and of utilizing virtual textures as stimuli in psychophysical experiments on texture perception. Conclusions drawn from the experiments reported here will be discussed with regard to these two application areas.

First, we concluded that the parameter space for stable haptic texture rendering using the PHANToM was too small to be useful, in the sense that only textures that felt like soft corduroy could be rendered without any artifacts. This result significantly restricts the types of surface textures that can be properly rendered in a virtual environment or a psychophysical study. Based on our results, many published studies may have used virtual textures that contained perceived instability. To what extent the results of these studies have been tainted by perceived instability is a question that needs to be carefully addressed.

Second, we found that stroking resulted in a larger stiffness threshold for stable texture rendering than static contact or poking (free exploration). This result is in favor of psychophysical experiments where subjects have to stroke the virtual surface in order to perceive its texture. Experimenters can explicitly prohibit subjects from pushing too deeply into the textured surface in order to preserve a stable rendering of the textures. In virtual environment applications, however, a user is usually allowed to explore object surfaces freely. The designer of virtual textures should therefore adhere to a more conservative parameter space for stable texture rendering.

Third, our measurements indicated that the frequency of the "buzzing" noise that contributed to perceived instability was quite intense (21.21–48.79 dB sensation level) at a relatively high frequency (192–240 Hz). In addition, measurements taken in our lab and others' revealed a mechanical resonance of the PHANToM devices at around 218 Hz. These results, along with the fact that texture rendering usually generates relatively fast changing force commands, stress the importance of considering the high-frequency behavior of a force-reflecting device, such as quantization noise of encoders and flexibility of joints and links, in both theoretical and experimental studies on stable texture rendering.

Fourth, we were able to predict (from texture model and user stroking velocity) and then locate (from our position, force, and acceleration measurements) the frequency components that conveyed texture information during the stroking mode. This frequency range was relatively low (26–65 Hz) and was well separated from the frequency range contributing to instability perception. We therefore believe that it should be possible to remove the high-frequency noise from proximal stimuli without affecting the components conveying texture information. Doing so will likely result in a significant increase of the parameter space for stable haptic texture rendering.

Finally, the perceived instability frequently observed in our experiments resulted from two sources of perceived instability: unstable control of the haptic interface, and inaccurate environment dynamics. Entry instability and inside instabilities, described as buzzing by the subjects, were due to the traditional control-related instability (e.g., mechanical resonance). Ridge instability occurred when force directions were varied based on only texture geometry and stylus position, without taking into account friction or user-applied force. Given the plethora of texture models that have been proposed, there is a pressing need for a better understanding of how these models and the associated rendering algorithms affect the perceived quality of haptic virtual textures. Our future work will continue to investigate the effect of inaccurate environment dynamics on the perceived instability of a haptic texture rendering system.

Acknowledgments

This work was supported in part by a National Science Foundation (NSF) Faculty Early Career Development (CAREER) Award under Grant 9984991-IIS, and in part by an NSF award under Grant 0098443-IIS. The authors wish to thank the anonymous reviewers for their insightful comments and suggestions on an earlier version of this manuscript.

References

Adams, R. J., & Hannaford, B. (1999). Stable haptic interaction with virtual environments. *IEEE Transactions on Robotics and Automation, 15*(3), 465–474.

Bolanowski, S. J., Jr., Gesheider, G. A., Verrillo, R. T., & Checkosky, C. M. (1988). Four channels mediate the mechanical aspects of touch. *Journal of Acoustical Society of America, 84*(5), 1680–1694.

Çavuşoğlu, M. C., Feygin, D., & Tendick, F. (2002). A critical study of the mechanical and electrical properties of the PHANToM haptic interface and improvements for high performance control. *Presence: Teleoperators and Virtual Environments, 11*(6), 555–568.

Choi, S., & Tan, H. Z. (2002a). An analysis of perceptual instability during haptic texture rendering. *Proceedings of the Tenth International Symposium on Haptic Interfaces for Virtual Environment and Teleoperator Systems,* 129–136.

———. (2002b). A study on the sources of perceptual instability during haptic texture rendering. *Proceedings of the IEEE International Conference on Robotics and Automation,* 1261–1268.

———. (2003). An experimental study of perceived instability during haptic texture rendering: Effects of collision detection algorithm. *Proceedings of the Eleventh International Symposium on Haptic Interfaces for Virtual Environment and Teleoperator Systems,* 197–204.

Costa, M. A., & Cutkosky, M. R. (2000). Roughness perception of haptically displayed fractal surfaces. *Proceedings of the ASME Dynamic Systems and Control Division, 69*(2), 1073–1079.

Fritz, J. P., & Barner, K. E. (1996). Stochastic models for haptic texture. *Proceedings of SPIE's International Symposium on Intelligent Systems and Advanced Manufacturing—Telemanipulator and Telepresence Technologies III,* 34–44.

Gescheider, G. A. (1985). *Psychophysics: Method, Theory, and Application* (2nd ed.). Mahwah, NJ: Erlbaum.

Gillespie, R. B., & Cutkosky, M. R. (1996). Stable user-specific haptic rendering of the virtual wall. *Proceedings of the ASME International Mechanical Engineering Congress and Exhibition, 58,* 397–406.

Hannaford, B., & Ryu, J.-H. (2002). Time-domain passivity control of haptic interfaces. *IEEE Transactions on Robotics and Automation, 18*(1), 1–10.

Hannaford, B., Ryu, J.-H., & Kim, Y. S. (2001). Stable control of haptics. In M. McLaughlin (Ed.), *Touch in Virtual Environments: Proceedings of USC Workshop on Haptic Interfaces* (pp. 47–70). Upper Saddle River, NJ: Prentice Hall.

Ho, C., Basdogan, C., & Srinivasan, M. A. (1999). Efficient point-based rendering techniques for haptic display of virtual objects. *Presence: Teleoperators and Virtual Environments, 8*(5), 477–491.

Hollerbach, J. M., & Johnson, D. E. (in press). Virtual environment rendering. *Human and Machine Haptics.*

Hollins, M., & Risner, S. R. (2000). Evidence for the duplex theory of tactile texture perception. *Perception & Psychophysics, 62,* 695–705.

Johnson, K. O., & Hsiao, S. S. (1992). Neural mechanisms of tactual form and texture perception. *Annual Review of Neuroscience, 15,* 227–250.

———. (1994). Evaluation of the relative roles of slowly and rapidly adapting afferent fibers in roughness perception. *Canadian Journal of Physiology & Pharmacology, 72,* 488–497.

Johnson, K. O., Yoshioka, T., & Vega-Bermudez, F. (2000). Tactile functions of mechanoreceptive afferents innervating the hand. *Journal of Clinical Neurophysiology, 17*(6), 539–558.

Katz, D. (1925/1989). *The world of touch.* Mahwah, NJ: Erlbaum.

Kim, L., Kyrikou, A., Sukhatme, G. S., & Desbrun, M. (2002). An implicit-based haptic rendering technique. *Proceedings of the IEEE/RSJ International Conference on Intelligent Robots and Systems,* 2943–2948.

Klatzky, R. L., & Lederman, S. J. (1999). Tactile roughness perception with a rigid link interposed between skin and surface. *Perception & Psychophysics, 61,* 591–607.

LaMotte, R. H., & Srinivasan, M. A. (1991). Surface microgeometry: Tactile perception and neural encoding. In O. Franzen & J. Westman (Eds.), *Information Processing in the Somatosensory Systems, Wenner-Gren International Symposium Series* (pp. 49–58). Houndmills, UK: MacMillan Press.

Lederman, S. J., & Klatzky, R. L. (1987). Hand movement: A window into haptic object recognition. *Cognitive Psychology, 19,* 342–368.

———. (1999). Sensing and displaying spatially distributed fingertip forces in haptic interfaces for teleoperator and virtual environment systems. *Presence: Teleoperators and Virtual Environments, 8,* 86–103.

Lederman, S. J., Klatzky, R. L., Hamilton, C. L., & Ramsay, G. I. (1999). Perceiving roughness via a rigid probe: Psychophysical effects of exploration speed and mode of touch. *Haptics-e* (http://www.haptics-e.org), *1*(1).

Lederman, S. J., & Taylor, M. M. (1972). Fingertip force,

surface geometry, and the perception of roughness by active touch. *Perception & Psychophysics, 12,* 401–408.

Massie, T. H. (1996). *Initial haptic explorations with the PHANToM: Virtual touch through point interaction.* Unpublished master's thesis, Massachusetts Institute of Technology, Cambridge.

Miller, B. E., Colgate, E., & Freeman, R. A. (2000). Guaranteed stability of haptic systems with nonlinear virtual environments. *IEEE Transactions on Robotics and Automation, 16*(6), 712–719.

Minsky, M., & Lederman, S. J. (1996). Simulated haptic textures: Roughness. *Proceedings of the ASME Dynamic Systems and Control Division, 58,* 421–426.

Minsky, M. D. R. (1995). *Computational haptics: The sandpaper system for synthesizing texture for a force-feedback display.* Unpublished doctoral dissertation, Massachusetts Institute of Technology, Cambridge.

Mountcastle, V. B., Talbot, W. H., Darian-Smith, I., & Kornhuber, H. H. (1955). Neural basis of the sense of flutter-vibration. *Science, 155,* 597–600.

Okamura, A. M., Dennerlein, J. T., & Howe, R. D. (1998). Vibration feedback models for virtual environments. *Proceedings of the IEEE International Conference on Robotics and Automation,* 674–679.

Siira, J., & Pai, D. K. (1996). Haptic texturing—A stochastic approach. *Proceedings of the IEEE International Conference on Robotics and Automation,* 557–562.

Smith, S. W. (1999). *The scientist and engineer's guide to digital signal processing* (2nd ed.). San Diego, CA: California Technical Publishing.

Tan, H. Z. (1996). *Information transmission with a multi-finger tactual display.* Unpublished doctoral dissertation, Massachusetts Institute of Technology, Cambridge.

Verrillo, R. T. (1963). Effect of contactor area on the vibrotactile threshold. *The Journal of the Acoustical Society of America, 35*(13), 1962–1966.

———. (1971). Vibrotactile thresholds measured at the finger. *Perception & Psychophysics, 9*(4), 329–339.

Verrillo, R. T., & Gescheider, G. A. (1992). Perception via the sense of touch. In I. R. Summers (Ed.), *Tactile aids for the hearing impaired* (pp. 1–36). London: Whurr Publishers Ltd.

Wall, S. A., & Harwin, W. S. (1999). Modeling of surface identifying characteristics using Fourier series. *Proceedings of the ASME Dynamic Systems and Control Division, 67,* 65–71.

———. (2000). Effects of physical bandwidth on perception of virtual gratings. *Proceedings of the ASME Dynamic Systems and Control Division, 69,* 1033–1039.

Weisenberger, J. M., Krier, M. J., & Rinker, M. A. (2000). Judging the orientation of sinusoidal and square-wave virtual gratings presented via 2-DOF and 3-DOF haptic interfaces. *Haptics-e* (http://www.haptics-e.org), *1*(4).